

FLARE: One-Shot PE-Level Fault Localization in Systolic Arrays via Algebraic Test Vectors

Logashree
Venkatasubramanian
Georgia Institute of Technology
School of Electrical and Computer
Engineering
Atlanta, Georgia, USA
lvenkata7@gatech.edu

Zishen Wan
Georgia Institute of Technology
School of Electrical and Computer
Engineering
Atlanta, Georgia, USA
zishenwan@gatech.edu

Viveck Cadambe
Georgia Institute of Technology
School of Electrical and Computer
Engineering
Atlanta, Georgia, USA
viveck@gatech.edu

Abstract

Systolic arrays are the dominant compute fabric for neural network inference. Prior work has addressed *column-level* fault detection efficiently with uniform test patterns, but *row-level* (PE-level) fault localization within a faulty column remains open without resorting to hardware redundancy. The fundamental obstacle is that uniform test inputs destroy per-row signatures: any test that activates every row equally cannot distinguish which row is the source of an observed deviation.

In this paper, we propose a lightweight, purely algorithmic remedy based on *coprime test vectors*. By assigning pairwise coprime integers as test-input entries, a permanent weight-register fault produces a deviation whose divisibility signature uniquely identifies the faulty row. Under a general bounded error model, a single test pass localizes the faulty row with high probability. This error model covers a broader class of faults than what prior dataflow-aware testing work has primarily emphasized. When one round is insufficient, a second pass using a ratio computation achieves exact localization; for the special case of single-bit errors, odd coprime entries guarantee exact localization in one round.

For INT16 arithmetic, a single test pass covers array sizes up to 256×256 with localization probability above 0.98, at a test cost under 1% of one inference GEMM tile.

Keywords

Systolic arrays, Fault localization, Coprime test vectors, Permanent faults, Algorithm-Based Fault Tolerance (ABFT), Online fault diagnosis, AI accelerator reliability

1 Introduction

Given the rapid growth of artificial intelligence workloads, particularly large language models, there has been a significant push toward designing power, performance, and area (PPA) efficient accelerators tailored to these workloads [1–4]. These accelerators are increasingly deployed in safety critical and time sensitive applications, including autonomous driving systems, space missions, medical robotics, and other embedded platforms where incorrect predictions can have severe consequences. Consequently, ensuring the reliability of AI accelerators has become a critical research challenge. Industry-scale studies from Google, Meta, and Alibaba reveal that silent data corruption (SDC), hardware faults producing incorrect results without error flags, occur at significant rates across major computing fleets, prompting dedicated teams at these

companies for fault detection and localization approaches [5, 6]. Permanent faults from latent manufacturing defects are of particular concern: such defects can escape post-silicon screening yet cause persistent silent data corruption in deployment [5–7]. Studies show that even a single faulty PE can meaningfully degrade DNN inference accuracy [8], making PE-level fault localization a critical prerequisite for targeted mitigation.

Systolic arrays have emerged as a dominant architectural paradigm for accelerating matrix intensive workloads, particularly in machine learning and deep neural networks [9, 10]. By organizing computation around a regular grid of Processing Elements (PEs), systolic arrays enable high throughput and energy efficient matrix multiplication, which forms the computational backbone of modern AI models. Industry grade AI accelerators, such as Google’s Tensor Processing Units (TPUs), are architected as large scale systolic arrays, highlighting the practical relevance of systolic array centric reliability challenges [1].

A common approach to fault tolerance relies on computational or hardware redundancy. Classical Algorithm Based Fault Tolerance (ABFT), initially proposed by Huang and Abraham [11], appends row and column checksums to input matrices and verifies computed outputs against these checksums to detect errors. Notably, ABFT incurs compute and memory overhead for checksum generation and verification, and the recovery step (when present) requires additional passes over the output. Hardware based approaches such as Double Modular Redundancy (DMR) or Triple Modular Redundancy (TMR) consume 100–200% additional area [12], directly undermining the PPA efficiency that makes systolic arrays attractive in the first place.

To preserve PPA while tolerating faults, recent work introduces spare PE rows or columns and reroutes computation around known faulty PEs [13–18]. These mitigation strategies, whether rerouting computation or adapting weight mappings to avoid faulty PEs [19], typically require the precise PE location as a prerequisite. Identifying the faulty PE requires taking the device offline and running diagnostic routines or BIST-based structural tests [5, 6, 20], or relying on dedicated hardware checkers, probes, or scan chains (including more recent augmented-array designs [21, 22]) that impose area and power overhead even when no faults are present. Recent algorithmic alternatives [23, 24] avoid this hardware cost by designing test patterns that expose faults during execution. However, they achieve only column-level fault detection using uniform test vectors, and cannot achieve *PE-level localization* — identifying which specific row within a faulty column contains the defective PE.

The core challenge is that systolic accumulation inherently destroys row-level identifiability: conventional test patterns collapse all row contributions into a single scalar, making localization impossible. In this paper, we develop a framework that actively designs input test vectors whose algebraic structure survives this accumulation, so that fault location can be obtained from the structure of the resulting output deviation. Our work addresses a complementary limitation of prior dataflow-aware testing approaches by enabling PE-level localization for weight-register faults without hardware augmentation.

Summary of Contributions. This work introduces a novel algorithmic framework to achieve *PE-level fault localization* in systolic arrays without hardware redundancy. We focus on permanent weight register (Wreg) faults in weight-stationary systolic arrays, the dominant dataflow in commercial AI accelerators where weights are retained locally within PEs to maximize data reuse and energy efficiency. Our key technical contribution is the development of carefully structured test vectors where fault deviations carry distinctive algebraic signatures that reveal both the location and magnitude of the underlying hardware defect. Our main contributions are as follows.

FLARE assumes at most one faulty weight register per column, with the error magnitude bounded within the representable precision range. Prior works such as RunSAFER [23] and Periodic Online Testing [24] validate only against single-bit stuck-at faults, whereas FLARE covers any error within this range, with single-bit faults as a special case.

Single-round structured localization: For an $L \times L$ systolic array performing b -bit integer computations, we develop a scheme where one test vector obtains the precise fault location with quantified probability, assuming at most one fault per column. Our framework uses pairwise coprime test vector entries to create unique divisibility signatures for each row. For INT16 computations, single-round localization covers typical accelerator array sizes ($L \leq 256$) with probability of successful localization above 0.98. Further, for permanent *single-bit* faults, our approach achieves exact localization in a single round, exploiting the power-of-two structure of these errors. This single-round result is particularly significant for safety-critical deployments where strict time budgets are allocated for fault detection (e.g., ISO 26262 specifies fault tolerant time interval (FTTI) constraints of 100–256 ms).

Two-round extension for complete coverage: When single-round localization is insufficient, a second test pass with a simple ratio computation achieves exact localization for all practical array sizes. This adapts the classical principle — familiar from ABFT and syndrome-based error correction — that two independent observations suffice to determine both the location and value of a single error.

Beyond localization, the framework estimates the magnitude of the hardware defect, enabling selective mitigation strategies where only significant faults affecting accuracy require correction. Thus, FLARE fills the critical gap between column-level detection and the localization requirements of fault-tolerant routing schemes, providing the precise faulty PE identification at run-time without hardware redundancy and minimal test overhead. We validate the

analytical bounds through fault injection experiments on a custom cycle-accurate systolic array simulator using weights from Qwen2.5-0.5B; empirical failure rates are consistent with the theoretical predictions across all tested array dimensions. Cycle overhead measured via SCALE-Sim stays at most 2 cycles per test round, below 0.1% of the cycles required for a single inference GEMM tile at 128×128 and 256×256 array sizes. We note that our results apply specifically to weight-register faults in weight-stationary dataflows; other fault types (e.g., input-register or MAC faults) exhibit different error structures and present a natural avenue for extending this framework.

Paper outline. Section 2 surveys prior work on ABFT, hardware redundancy, dataflow aware testing, silent data corruption, and DNN resilience under faults. Section 3 states the system and fault models and presents the formal problem formulation. Section 4 presents the FLARE one round and two round fault localization algorithms, along with formal theorems that bound the probability of successful localization as a function of array dimension and compute precision. Section 5 instantiates FLARE for INT8 and INT16, validates the analytical bounds through fault injection experiments on a custom systolic array simulator, and characterizes the cycle overhead using SCALE-Sim.

2 Related Work

2.1 Fault Detection and Correction

Algorithm-Based Fault Tolerance (ABFT) [11] augments computation with checksum redundancy to detect and correct errors at the output. Subsequent work reduces overhead and adapts ABFT to modern workloads, including efficient encoding for systolic arrays [25–27], and approximate variants for quantized inference [28] and layer-specific schemes for transformers [29, 30]. Statistical methods have also been used to selectively protect vulnerable layers in LLM inference [31]. These approaches are effective for transient faults, where correcting the output suffices.

ABFT operates at the output level and cannot localize faults to the PE level; hardware approaches achieve PE-level localization but incur area overhead. Our work bridges this gap with an algorithmic solution that delivers PE-level localization without hardware augmentation.

Arithmetic (AN) and residue codes [32, 33] also introduce algebraic redundancy to detect computation errors via consistency checks. These approaches use coprime and modular structure with the goal of invariant checking, whereas our goal is fault localization. While AN and residue codes bear some high level resemblance with our test vector constructions, we see no direct technical connection between the two approaches.

2.2 Dataflow-Aware Testing and Localization

An alternative to output-level detection is to exploit systolic dataflow to design test inputs that expose faults. RunSAFER [23] and Periodic Online Testing [24] inject structured (often uniform) test patterns to detect faults during execution, but achieve only coarse-grained localization at the column level. More broadly, prior work [34, 35] emphasizes runtime detection mechanisms compatible with accelerator datapaths, similarly limited to column or module-level granularity.

Table 1: Comparison of dataflow-aware fault testing approaches for weight-stationary systolic arrays.

	RunSAFER [23]	Periodic Online Testing [24]	HW-Runtime [21]	FLARE (this work)
Fault model (validated)	single-bit stuck-at	single-bit stuck-at	single-bit stuck-at	bounded error (any $ e \leq M$)
Test overhead (cycles)	2	4	$4 \times$ array-size	1 or 2
Localization	PE col	PE col	PE row & col	PE row & col, $ e $
Hw. modif.	no	no	yes	no
Error est.	no	no	no	yes

This limitation arises from the accumulation inherent in weight-stationary dataflow. Each column computes $y_j = \sum_i w_{ij} x_i$, so uniform inputs (e.g., all-ones) cause all rows to contribute equally. As a result, row-level information is lost, and the observed deviation indicates only that *some* PE in the column is faulty. Achieving PE-level localization therefore requires test inputs that preserve distinct per-row signatures. This is precisely the gap addressed by our approach.

Offline structural testing, scan-chain-based diagnosis [20, 22], and hardware-augmented runtime approaches [21] can all achieve PE-level localization, but each requires dedicated hardware: for instance, HW-Runtime [21] augments the array with spare PEs, a control hub, and on-chip comparators, incurring approximately 1.74% area overhead for a 256×256 array. ML-based frameworks such as DiagNNose [36] offer architecture-specific fault attribution but require fault injection campaigns to generate training data. Across all these approaches, the focus has been limited to single-bit stuck-at faults [21, 23, 24].

Single-bit faults produce an error that is always a power of two. While the underlying detection mechanisms of previous works may be useful for multi-bit or arbitrary faults, formal guarantees for such settings have not been established. Importantly, real hardware faults may produce arbitrary bounded errors due to multi-bit defects, bridging faults, or parametric variation. In contrast to previous work, our framework explicitly considers such general faults via a general bounded error model ($|e| \leq M$), subsuming single-bit faults as a special case. When the error is a single-bit fault, our method provides strictly stronger guarantees (exact localization in one round) as listed in Table 1. For weight-register faults, FLARE achieves the same localization granularity as HW-Runtime with no hardware overhead and fewer test runs under a more general fault model. In contrast to prior approaches, FLARE also detects the exact deviation of the weight register and can therefore potentially enable selective mitigation strategies (Sec. 2.3). As noted in the introduction, existing methods [21, 23, 24] target broader fault classes beyond weight-register faults, specifically input-register, MAC, and accumulator register faults. The task of advancing the key conceptual insight of FLARE – that carefully designing algebraic test vectors tailored to the fault model can provide efficient fault localization – to models beyond weight-register faults is an open research direction motivated by our paper.

2.3 DNN Resilience and Fault Impact

Large-scale studies of silent data corruption (SDC) [5, 6] show that existing systems can detect that errors occur but typically cannot localize their origin. In systolic-array-based accelerators, prior work has also analyzed the impact of permanent faults on inference

accuracy and proposed mitigation strategies such as retraining or redundancy [8].

DNN inference exhibits inherent resilience to hardware faults, particularly for low-order bit errors [37–40]. The impact of a fault depends strongly on its magnitude and location: high-order bit errors (e.g., sign or MSB) can significantly degrade accuracy, while low-order perturbations often have negligible effect. Sensitivity also varies across layers and parameters [41–43], motivating selective protection strategies that focus on the most critical components.

To quantify fault impact, the Parameter Vulnerability Factor (PVF) [44] identifies which model parameters most affect inference accuracy when corrupted. However, PVF does not indicate where the fault originates in hardware. Low-cost runtime monitoring approaches [45] can detect such corruptions with minimal overhead, but do not localize the fault source. Our framework complements such analysis by localizing the faulty PE and estimating the error magnitude, enabling targeted mitigation that prioritizes high-impact faults while avoiding unnecessary correction.

3 System Model and Fault Model

3.1 Weight-Stationary Systolic Array

An $L \times K$ systolic array contains $L \cdot K$ processing elements (PEs) arranged in a grid. PE(i, j), with $i \in [L]$ and $j \in [K]$, holds three components:

- (1) a *weight register* (Wreg), storing a signed integer w_{ij} ;
- (2) an *input register* (Ireg), receiving the signed integer activation x_i that flows from left to right across row i ;
- (3) a *multiply-accumulate unit* (MAC), computing $w_{ij} \cdot x_i$ and adding to a partial sum flowing top-to-bottom in column j .

Given input $\mathbf{x} = (x_1, \dots, x_L)^T$, column j produces

$$y_j = \sum_{i=1}^L w_{ij} x_i, \quad j = 1, \dots, K. \quad (1)$$

Both Wreg and Ireg operands are *signed* b -bit integers in $\{-2^{b-1}, \dots, 2^{b-1} - 1\}$ (two’s complement); the accumulator is wider (e.g. 32 bits), so (1) incurs no overflow. Throughout, “INT b ” refers to the signed b -bit representation.

3.2 Fault Model

We focus on permanent weight-register faults in weight-stationary systolic arrays. In this dataflow, each PE stores a weight value that persists for the duration of a tile computation. A permanent defect in the weight register produces a deviation with a multiplicative structure that our algebraic framework exploits. Regardless of the physical fault mechanism, a permanent Wreg fault in PE(i^*, j^*) can be modeled as an additive perturbation to the stored weight:

$$\tilde{w}_{i^* j^*} = w_{i^* j^*} + e, \quad \Delta_{j^*} \triangleq \tilde{y}_{j^*} - y_{j^*} = e \cdot x_{i^*}, \quad (2)$$

with $\Delta_j = 0$ for $j \neq j^*$.¹ We analyze two error models for e .

¹A stuck-at fault produces $e \neq 0$ only when the loaded weight disagrees with the stuck bit; otherwise the fault is *masked*. Ensuring activation (i.e., $e \neq 0$) is a standard test-engineering concern addressed by loading complementary weight patterns such as all-zeros and all-ones. Our framework assumes the fault is activated ($e \neq 0$) and focuses on localizing the faulty row from the observed deviation.

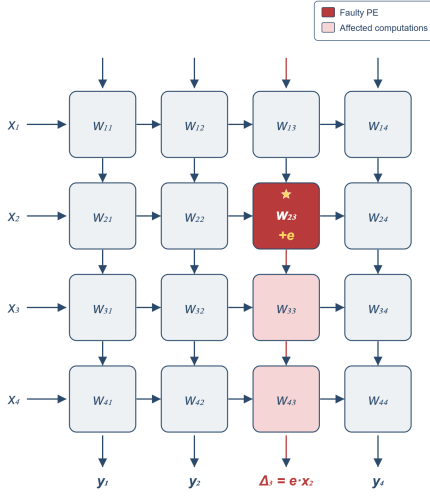


Figure 1: Error propagation pattern for a Wreg fault in a 4×4 weight-stationary systolic array, where a fault adds a persistent error e that corrupts every MAC involving that PE.

Bounded error model. For general faults (multi-bit defects, bridging faults, parametric drift, or silent data corruption) we make no assumption on the error value beyond a magnitude bound:

$$e \sim \text{Uniform}(\{1, \dots, M\}), \quad M = 2^{b-1} - 1. \quad (3)$$

This is the primary model under which we state all main results.

Single-bit-error model. We also analyze our algorithms under a structured special case of the bounded error model: a permanent defect that forces bit β of the weight register to a fixed value $v \in \{0, 1\}$, regardless of the data written, produces an error

$$e = \pm 2^\beta, \quad (4)$$

a signed power of two, whenever the intended weight has bit β equal to $1-v$; otherwise the fault is *masked* ($e = 0$). Because single-bit errors have the restricted form $e = \pm 2^\beta$, our coprime scheme achieves strictly stronger guarantees than under the general bounded error model; we highlight these as remarks following the main theorems.

We state the main results under the bounded error model: Theorem 2 gives a one round probabilistic guarantee, and Section 4.4 presents a two round ratio-based scheme for exact localization when one round is insufficient. For the single-bit-error model, Remark 3 notes that exact localization in a single round is achievable.

Assumptions.

(A1) At most one PE per column has a permanent fault.

(A2) $1 \leq |e| \leq M = 2^{b-1} - 1$.

(A3) The faulty column is identified by $\Delta_{j^*} \neq 0$.

Notably, we restrict attention to *weight-register* faults, which result in the multiplicative structure (2) that enables the algebraic localization techniques of our paper.

3.3 Problem Statement

Consider a test phase in which a known weight matrix W has been loaded into the array and a fixed test input vector \mathbf{x} is applied. The expected output $\mathbf{y} = W^T \mathbf{x}$ is precomputed offline. If a permanent Wreg fault corrupts PE(i^*, j^*), the observed output $\hat{\mathbf{y}}$ differs from \mathbf{y}

Table 2: Notation.

L, K	rows, columns of systolic array
b	operand bit-width
M	$2^{b-1} - 1$; max signed magnitude
e	additive error from Wreg fault
Δ_j	output deviation of column j
$\mathbf{x} = (x_1, \dots, x_L)^T$	test vector; entries pairwise coprime
$\pi(M)$	Prime Counting Function: The number of prime numbers smaller than or equal to M
P_{fail}	probability that localization is incomplete after one round

in column j^* by $\Delta_{j^*} = e \cdot x_{i^*}$ (Eq. 2), while all other columns match exactly. *Detecting* that a fault has occurred is therefore straightforward: any $\hat{y}_j \neq y_j$ signals a faulty column.

The harder problem and the focus of this paper is *localization*: identifying *which row i^** within the faulty column contains the defective PE, and recovering the error value e .

Since each column computes an independent inner product (1) and a Wreg fault affects only column j^* , the localization problem decomposes across columns. It therefore suffices to consider a single column with weight vector $\mathbf{w} = (w_1, \dots, w_L)^T$, expected output $y = \mathbf{w}^T \mathbf{x}$, and observed output $\hat{y} = y + e \cdot x_{i^*}$. We adopt this single-column notation for the remainder. Formally:

Row Localization Problem. Design a small set of test input vectors $\mathbf{x}^{(1)}, \dots, \mathbf{x}^{(R)} \in \{-M, \dots, M\}^L$, each with entries $\mathbf{x}^{(r)} = (x_1^{(r)}, \dots, x_L^{(r)})^T$, such that from the observed deviations $\Delta^{(r)} = e \cdot x_{i^*}^{(r)}$ ($r = 1, \dots, R$), the faulty row i^* and error e can be recovered exactly or with miss probability bounded by Theorem 2. Table 2 lists notation.

4 Coprime Test-Vector Fault Localization

The scheme developed in this section is organized around a central idea: encoding fault location into arithmetic structure so that a small number of test passes recovers the faulty row from the observed deviation. We begin with a worked example (Section 4.1) and formalize the general framework (Section 4.2). Section 4.3 presents our main result: a *single-round* construction based on pairwise coprime divisibility signatures, with a precise bound on the probability of successful localization (Theorem 2). Section 4.4 then develops a complementary two round construction that achieves exact localization. The two round construction serves two purposes: it provides exact localization as a fallback when one round is insufficient, and it offers a reference point against which the single-round result can be contrasted. Section 4.5 quantifies the test overhead for both schemes.

4.1 Motivating Example

Before stating the general framework, we trace through a small instance that illustrates every step.

Example 1 (Signed INT4, $L = 4$). Consider a single column with $L = 4$ rows, signed $b = 4$ -bit operands ($M = 2^{b-1} - 1 = 7$), and weight vector $\mathbf{w} = (w_1, w_2, w_3, w_4)^T$. Assign pairwise coprime test-vector entries, here the four primes ≤ 7 : $\mathbf{x} = (7, 5, 3, 2)^T$. The expected output is $y = 7w_1 + 5w_2 + 3w_3 + 2w_4$.

Symbolic deviation. If row $i^* = 2$ has a Wreg fault with error e , the observed output is

$$\hat{y} = 7w_1 + 5(w_2 + e) + 3w_3 + 2w_4 = y + 5e,$$

giving deviation $\Delta = \hat{y} - y = 5e = e \cdot p_2$.

Concrete instance. Load the all-ones test weight pattern $\mathbf{w} = (7, 7, 7, 7)^T$, so $y = 7(7+5+3+2) = 119$. A single-bit error on bit 2 of w_2 (bit forced to 0) changes $w_2 = 7 = 0b0111$ to $0b0011 = 3$, giving $e = 3 - 7 = -4$. The observed output is $\hat{y} = 119 + 5 \cdot (-4) = 99$, so $\Delta = 99 - 119 = -20$.

Localization. For each row k , test whether $x_k \mid \Delta$ and check the implied error magnitude, which must satisfy $|e| \leq M = 7$ since operands are limited to $b = 4$ -bit precision:

Row k	x_k	$x_k \mid -20?$	Δ/x_k	$ \Delta/x_k \leq 7?$
1	7	No	—	—
2	5	Yes	-4	Yes ✓
3	3	No	—	—
4	2	Yes	-10	No

Row 2 is the unique candidate: the scheme correctly localizes the fault and recovers $e = -4$. Row 4 passes the divisibility test ($2 \mid 20$) but is eliminated by the magnitude check ($|-10| > 7$).

This example illustrates that localization reduces to identifying which test vector entry divides the residual while respecting magnitude constraint. Two features are worth noting:

- (1) **Why pairwise coprime?** The deviation $\Delta = e \cdot c_{i^*}$ is a product of two factors. Because the entries are pairwise coprime ($\gcd(c_k, c_{i^*}) = 1$ for $k \neq i^*$), a “wrong” entry c_k can divide Δ only if it divides the error e itself. That is, row k survives the divisibility test only if c_k divides e . Depending on the error model, we can bound the likelihood of the error e being divisible by the wrong entry, which leads to the likelihood of localization with one test vector.
- (2) **Power-of-two errors.** Single-bit errors produce errors $e = \pm 2^\beta$, which are powers of two. No odd integer coprime to 2 divides a power of two, so if we restrict to odd coprime entries, a single-bit error is localized *with certainty* in a single round. We formalize this below.

4.2 General Framework

The test vector $\mathbf{x} = (x_1, \dots, x_L)^T$ has entries that are *pairwise coprime*: $\gcd(x_i, x_j) = 1$ for all $i \neq j$. Recall from Section 3.3 that we work with a single column: a fault in row i^* with error e produces deviation $\Delta = e x_{i^*}$. The localization procedure checks, for each candidate row k , whether $x_k \mid \Delta$. If row $k \neq i^*$ also passes this test, localization is incomplete: multiple candidate rows survive.

PROPOSITION 1 (COPRIME DIVISIBILITY TEST). *Let \mathbf{x} have pairwise coprime entries x_1, \dots, x_L . Suppose the fault is in row i^* with error $e \neq 0$. Then row $k \neq i^*$ survives the divisibility test if and only if $x_k \mid e$. In particular, if e is not divisible by x_k for any $k \neq i^*$, then i^* is the unique survivor and localization is complete.*

PROOF. Row k survives the divisibility test iff $x_k \mid \Delta = e x_{i^*}$. Since $\gcd(x_k, x_{i^*}) = 1$, this holds if and only if $x_k \mid e$. \square

Algorithm 1: Single-Vector Coprime Localization

Input: L, K, M ; weight matrix W
Output: candidate set C_j for each faulty column j

- 1 Set $x_k \leftarrow$ the k -th largest prime $\leq M$, for $k = 1, \dots, L$;
- 2 $\mathbf{x} \leftarrow (x_1, \dots, x_L)^T$;
- 3 **foreach** column $j \in [K]$ **do**
- 4 $y_j^{\text{exp}} \leftarrow \sum_i w_{ij} x_i$;
- 5 **end**
- 6 Stream \mathbf{x} through the systolic array; observe y_j^{obs} ;
- 7 **foreach** column j **do**
- 8 $\Delta_j \leftarrow y_j^{\text{obs}} - y_j^{\text{exp}}$;
- 9 **if** $\Delta_j \neq 0$ **then**
- 10 $C_j \leftarrow \{(k, \Delta_j/x_k) : x_k \mid \Delta_j, |\Delta_j/x_k| \leq M\}$;
- 11 **end**
- 12 **end**

Algorithm 1 additionally checks the magnitude condition $|\Delta/x_k| \leq M$, which can eliminate candidates that pass the divisibility test but imply an error exceeding the representable range (as seen for row 4 in Example 1).²

A key design implication of Proposition 1: since row k survives the divisibility test only if $x_k \mid e$, and the number of multiples of x_k in $\{1, \dots, M\}$ is $\lfloor M/x_k \rfloor$, *larger entries reduce the number of surviving candidates*. For example, an entry $x_k = 113$ has only $\lfloor 127/113 \rfloor = 1$ multiple in $\{1, \dots, 127\}$, while $x_k = 2$ has 63 multiples. This motivates choosing entries as large as possible.

An important constraint on the test vector length follows from pairwise coprimality. If x_1, \dots, x_L are pairwise coprime integers with $x_k \leq M$ for all k , then each x_k must contain at least one prime factor not shared with any other entry, and all such prime factors are $\leq M$. Therefore $L \leq \pi(M)$, where $\pi(\cdot)$ denotes the prime-counting function (the number of primes up to its argument). The constraint $L \leq \pi(M)$ highlights a fundamental tradeoff: fault localization for larger arrays requires either additional probes or larger input magnitudes.

4.3 One-Round Localization ($L \leq \pi(M)$)

When $L \leq \pi(M)$, a single test vector with L pairwise coprime entries suffices. To maximize $\min_k x_k$, we choose the L largest primes $\leq M$, though any set of L pairwise coprime integers $\leq M$ would work. Algorithm 1 gives the procedure.

We now state the localization guarantees.

THEOREM 2 (PROBABILITY THAT LOCALIZATION IS INCOMPLETE AFTER ONE ROUND). *Let $L \leq \pi(M)$ and assign pairwise coprime entries $x_1, \dots, x_L \leq M$. Under the bounded error model with e uniform on $\{1, \dots, M\}$, the average probability that localization is incomplete after one round satisfies*

$$P_{\text{fail}} \leq \frac{L-1}{LM} \sum_{k=1}^L \lfloor M/x_k \rfloor. \quad (5)$$

²The analysis throughout uses only the divisibility condition $x_k \mid e$ and ignores the magnitude check. Since the magnitude check can only eliminate candidates, the stated bounds are conservative; a refined analysis incorporating this condition can only improve them.

When all entries exceed $M/2$, each $\lfloor M/x_k \rfloor = 1$ and this simplifies to $P_{\text{fail}} \leq (L-1)/M$.

PROOF. By Proposition 1, row $k \neq i^*$ survives the divisibility test iff $x_k \mid e$. The number of $e \in \{1, \dots, M\}$ divisible by x_k is $\lfloor M/x_k \rfloor$, so $\Pr(x_k \mid e) = \lfloor M/x_k \rfloor / M$. By the union bound, $P_{\text{fail}}(i^*) \leq \frac{1}{M} \sum_{k \neq i^*} \lfloor M/x_k \rfloor$. Averaging over i^* : each term $\lfloor M/x_k \rfloor$ appears in exactly $L-1$ of the L inner sums (excluded only when $i^* = k$), giving $P_{\text{fail}} \leq \frac{L-1}{LM} \sum_{k=1}^L \lfloor M/x_k \rfloor$. \square

Theorem 2 has two practical implications. First, it reinforces the design principle from Proposition 1: each term $\lfloor M/x_k \rfloor$ shrinks as x_k grows, so choosing the largest available pairwise coprime entries minimizes the bound. Second, the bound improves sharply with operand bit-width. As b (equivalently M) grows, the prime pool $\pi(M)$ expands, and for any fixed array size L one can eventually select L pairwise coprime entries all exceeding $M/2$. In this regime the bound collapses to the simplified form $P_{\text{fail}} \leq (L-1)/M$, which vanishes as $M \rightarrow \infty$. We explore this in Section 5 where we instantiate our results for INT8 and INT16.

Remark 3 (Single-bit errors: exact single-round localization). Under the single-bit-error model ($e = \pm 2^\beta$), if all entries x_k are chosen as the L largest odd primes $\leq M$ (requiring $L \leq \pi(M) - 1$), then $x_k \nmid e$ for every $k \neq i^*$, since $|e|$ is a power of two and every $x_k \geq 3$ is odd. By Proposition 1, no other row survives the divisibility test and the faulty row is identified exactly with a single test vector.

4.4 Ratio-Based Two-Round Localization

The one round scheme of Section 4.3 leaves two cases unresolved. First, for $L \leq \pi(M)$, round 1 localizes with miss probability bounded by Theorem 2 but not with certainty: a fraction of faults produce errors e that are not localized in one round. Second, for $L > \pi(M)$, a single test vector cannot have all entries pairwise coprime, and one round localization is not directly applicable. We now present a two round scheme that resolves both cases. It serves as a *fallback* for round-1 failures when $L \leq \pi(M)$ and as the *primary* localization method when $L > \pi(M)$.

Given two test vectors $\mathbf{x}^{(1)}$ and $\mathbf{x}^{(2)}$ with row entries $x_k^{(1)}$ and $x_k^{(2)}$, a fault in row i^* with error e produces deviations

$$\Delta^{(1)} = e \cdot x_{i^*}^{(1)}, \quad \Delta^{(2)} = e \cdot x_{i^*}^{(2)}. \quad (6)$$

Taking the ratio cancels the error magnitude entirely:

$$\frac{\Delta^{(2)}}{\Delta^{(1)}} = \frac{x_{i^*}^{(2)}}{x_{i^*}^{(1)}}. \quad (7)$$

The key idea of the two round localization algorithm is to design test vectors so that every row has a distinct reduced ratio $r_k = x_k^{(2)}/x_k^{(1)}$, the observed ratio identifies the faulty row unambiguously. The error is then recovered by a single integer division, $e = \Delta^{(1)}/x_{i^*}^{(1)}$.

Feasibility constraint. Identification by ratio requires the per-row reduced ratios r_k to be pairwise distinct. Since both $x_k^{(1)}$ and $x_k^{(2)}$ live in $\{1, \dots, M\}$, the number of representable distinct ratios is finite. The set of admissible reduced ratios is

$$\mathcal{F}_M = \{p/q : 1 \leq p, q \leq M, \gcd(p, q) = 1\}, \quad (8)$$

the set of all distinct reduced fractions with numerator and denominator in $\{1, \dots, M\}$.³ The ratio scheme therefore supports

$$L \leq |\mathcal{F}_M| \approx \frac{6}{\pi^2} M^2. \quad (9)$$

For INT8 this gives about 9800; for INT16, on the order of 6.5×10^8 . This is a theoretical upper bound; the two instantiations presented below do not saturate it but cover all array sizes of practical interest. The principle that two independent observations suffice to determine one error's location and value is classical, appearing in ABFT checksum schemes [11] and in syndrome-based error correction [47]. Its application to PE-level fault localization in systolic arrays, along with the implied bounds (9), appears to be new. We present two useful instantiations: one for the case where it is used as a fallback for small array sizes to complement the one round test, and another for larger array sizes.

Instantiation 1: Derangement of primes (fallback for $L \leq \pi(M)$). Let $\mathbf{x}^{(1)} = (x_1, x_2, \dots, x_L)$ be the round-1 test vector, whose entries are pairwise coprime. Let σ be a derangement of $\{1, \dots, L\}$ (a permutation with no fixed points, $\sigma(k) \neq k$), and set $\mathbf{x}^{(2)} = (x_{\sigma(1)}, x_{\sigma(2)}, \dots, x_{\sigma(L)})$. Derangements exist for all $L \geq 2$, so this construction covers any $L \in [2, \pi(M)]$. The fact that the x_1, x_2, \dots, x_k are pairwise coprime implies that the ratios $\frac{x_k}{x_{\sigma(k)}}$ are all distinct. Critically, $\mathbf{x}^{(1)}$ is exactly the round-1 vector, so this instantiation is the natural fallback: if round 1 already localizes, the second pass is skipped; otherwise the second pass with $\mathbf{x}^{(2)}$ resolves the residual ambiguity via ratio recovery.

Instantiation 2: Consecutive integers (primary for $L > \pi(M)$). Let $\mathbf{x}^{(1)} = (1, 2, 3, \dots, L)$ and $\mathbf{x}^{(2)} = (L, 1, 2, \dots, L-1)$. The row pairs are $(1, L)$ and $(k, k-1)$ for $k = 2, \dots, L$. Consecutive integers are coprime ($\gcd(k, k-1) = 1$ and $\gcd(1, L) = 1$), and the L ratios $L, 1/2, 2/3, \dots, (L-1)/L$ are pairwise distinct. The construction requires $L \leq M$ and uses no primes at all. This covers all practical array sizes at INT8 and above: $L \leq 127$ at INT8 and $L \leq 32767$ at INT16. For the slice between M and the bound $|\mathcal{F}_M|$ in (9), any enumeration of reduced fractions in \mathcal{F}_M suffices.

Example 2 (Ratio-based two round localization, signed INT4, $L = 7$). Consider $L = 7$ rows with $b = 4$ ($M = 7$). Since $\pi(7) = 4 < 7$, one round is insufficient.

Applying Instantiation 2:

$$\mathbf{x}^{(1)} = (1, 2, 3, 4, 5, 6, 7)^T \text{ and } \mathbf{x}^{(2)} = (7, 1, 2, 3, 4, 5, 6)^T.$$

Row 1 receives the pair $(1, 7)$; rows $k = 2, \dots, 7$ receive $(k, k-1)$. The ratios are $7, 1/2, 2/3, 3/4, 4/5, 5/6, 6/7$ — all distinct. Suppose row $i^* = 3$ has a fault with error $e = -2$.

Round 1. $\Delta^{(1)} = e \cdot x_3^{(1)} = (-2) \cdot 3 = -6$.

Round 2. $\Delta^{(2)} = e \cdot x_3^{(2)} = (-2) \cdot 2 = -4$.

Ratio recovery. $\Delta^{(2)}/\Delta^{(1)} = (-4)/(-6) = 2/3$, which matches row 3 uniquely (pair $(3, 2)$). The error is recovered as $e = \Delta^{(1)}/x_3^{(1)} = -6/3 = -2$.

³This set is closely related to the Farey sequence of order M . Its cardinality equals the number of coprime pairs (p, q) with $1 \leq p, q \leq M$, which is $2 \sum_{q=1}^M \phi(q) - 1$ where ϕ is the Euler totient function. A classical result in number theory [46] gives $\sum_{q=1}^M \phi(q) \sim 3M^2/\pi^2$, yielding $|\mathcal{F}_M| \approx 6M^2/\pi^2$.

4.5 Integration and Overhead

The localization scheme requires no new PE hardware or dedicated test datapaths. A test pass is a standard matrix-vector multiply through the existing array: the current weight tile stays resident in the PEs, the coprime sketch vector is presented as a normal activation column, and the output is read back through the standard output interface. The golden checksum $\mathbf{c} = W_{\text{gold}} \mathbf{x}$ is a small per-tile precomputation stored alongside the weight tile in memory and fetched on demand. Post-processing runs on the array controller: compute $\Delta = \mathbf{s} - \mathbf{c}$, scan for the nonzero entry to find the faulty column j^* , then run $O(L)$ divisibility checks to locate the faulty row i^* . This is $O(L \log M)$ bit operations in total: the $O(L)$ divisibility checks each cost $O(\log M)$ bit operations since every operand has $O(\log M)$ bits, keeping the total negligible relative to the array passes.

Deployment follows the same pattern as RunSAFER [23]: the test is defined as an ISA instruction that queues the sketch vector(s) into the activation pipeline alongside normal inference traffic. Whether the trigger originates from an ISA opcode, a runtime scheduler, or a host driver call is a deployment choice; the array-level operations are identical in all cases. The ISA path is the natural production choice because it gives the controller deterministic timing. Since the sketch vector is $1 \times L$, it matches the pipeline width exactly and is absorbed in one cycle with no stalls. As shown in Section 5.2.2, the incremental cost of issuing a sketch vector through an already-loaded array is exactly 1 cycle regardless of array size, making the overhead inherently negligible.

5 Evaluation

We evaluate FLARE along two axes: analytical characterization of localization probability, and empirical validation via fault-injection simulation. For the analytical part we instantiate the P_{fail} bounds of Theorem 2 for INT8 and INT16, comparing raw-prime and prime-power coprime pool constructions. For the empirical part we validate these bounds on a custom cycle-accurate systolic array simulator and measure cycle overhead with SCALE-Sim 3.0.0 [10], reporting the incremental cost over a baseline of one inference tile without the sketch vector. Array dimensions are chosen to include the 128×128 and 256×256 configurations of the Google TPU [1] as reference deployment targets.

5.1 Analytical Results

We instantiate the P_{fail} bounds of Theorem 2 for INT16 and INT8, comparing the raw-prime and prime-power coprime pool constructions for each.

5.1.1 INT16 ($b = 16, M = 32767$). At INT16 the prime pool is $\pi(32767) = 3512$, and 1612 of these primes exceed $M/2$. Assigning the L largest primes to the rows, the simplified bound $P_{\text{fail}} \leq (L - 1)/M$ from Theorem 2 therefore applies for all $L \leq 1612$, which covers the 128×128 and 256×256 array dimensions of the Google TPU [1]. For $L = 256$ this evaluates to under 0.008, and for $L = 1024$ to under 0.032. The single-round scheme (Algorithm 1) suffices at INT16 with no need for the prime-power construction or two round fallback developed for INT8 below. Under the single-bit-error model

(Remark 3), restricting to odd primes yields exact single-round localization.

5.1.2 INT8 ($b = 8, M = 127$). The 31 primes ≤ 127 are

2, 3, 5, 7, 11, 13, 17, 19, 23, 29, 31, 37, 41, 43, 47,
53, 59, 61, 67, 71, 73, 79, 83, 89, 97, 101, 103, 107, 109, 113, 127.

Bounded error model. Using all 31 primes, Theorem 2 gives the average P_{fail} via (5). The 13 largest primes all exceed $M/2 = 63$; each contributes $\lfloor M/x_k \rfloor = 1$. Evaluating (5):

L	primes used	P_{fail} (Theorem 2)
8	{89, ..., 127}	$\leq 7/127 \approx 0.055$
16	{53, ..., 127}	$\leq 15/127 \approx 0.118$
31	all (prime-power)	$\leq 2100/3937 \approx 0.534$

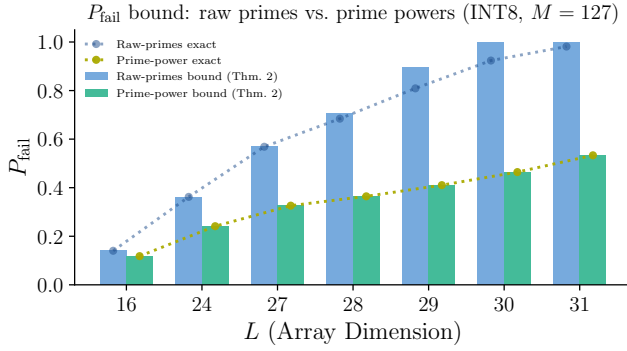
Sharper construction: prime powers as coprime entries. One round construction of Section 4.3 and the corresponding analysis of Theorem 2 requires only that the test entries be *pairwise coprime*, not that they be prime. This freedom can be exploited: each small prime p can be replaced by the largest power $p^k \leq M$ that fits in the error domain, without violating coprimality (since each power involves only one prime base). For $M = 127$ the replacements are

$$2 \rightarrow 2^6 = 64, \quad 3 \rightarrow 3^4 = 81, \quad 5 \rightarrow 5^3 = 125, \\ 7 \rightarrow 7^2 = 49, \quad 11 \rightarrow 11^2 = 121$$

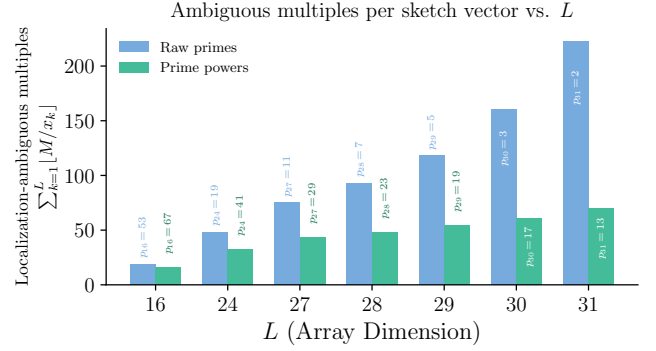
while primes ≥ 13 remain unchanged. The resulting pool still has $\pi(127) = 31$ entries, but the smallest entry rises from 2 to 13. The number of multiples in $\{1, \dots, 127\}$ collapses dramatically: where the original prime 2 contributed 63 multiples, 64 contributes only $\lfloor 127/64 \rfloor = 1$. Similarly 81, 125, 121 each contribute only one multiple, and 49 contributes two. Substituting into Theorem 2 reduces P_{fail} for $L = 31$ from impractical (the small primes dominate the union bound) to $2100/3937 \approx 0.534$. Figure 2 shows the empirical impact: for a single sketch vector applied to INT8 ($M = 127$), the prime power pool produces a noticeably lower average P_{fail} than the raw prime pool, with the gap widening beyond $L = 27$ where the raw prime pool is forced to include the small primes (11, 7, 5, 3, 2) that dominate the union bound.

The union bound of Theorem 2 overcounts when e is divisible by multiple pool entries, as with the raw-prime pool where entries like 2 and 3 share common multiples in $\{1, \dots, M\}$; the exact P_{fail} (Appendix A) corrects for this and falls strictly below the bound. The prime-power pool eliminates this overcounting: since no two entries share a common multiple in $\{1, \dots, M\}$, the bound coincides with the exact P_{fail} computation for prime-power pool entries (Figures 2a and 3). Beyond tightness, the union bound evaluates in $O(L \log M)$ bit operations (Section 4.5), whereas the exact P_{fail} via inclusion-exclusion (Appendix A) scales exponentially in L and becomes impractical for large arrays. We therefore use the Theorem 2 bound with the prime-power pool throughout, as it matches the exact P_{fail} and remains a tight estimate across all tested dimensions.

Production-scale arrays ($L \in \{128, 256\}$). For $L > 31 = \pi(127)$, the one round scheme cannot assign a unique coprime entry to every row. The ratio-based two round scheme (Section 4.4) provides exact localization for almost all practical INT8 array sizes, since $|\mathcal{F}_{127}| \approx 9,800$ (Eq. 9) far exceeds most production array dimensions.

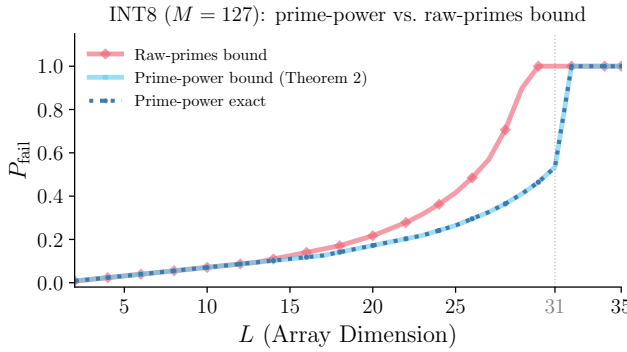


(a) Average P_{fail} bound (Theorem 2) for raw primes and prime powers. The prime-power exact value coincides with its bound, confirming no overcounting. The raw-prime exact value falls below its bound, showing the union bound overcounts when small primes are present.

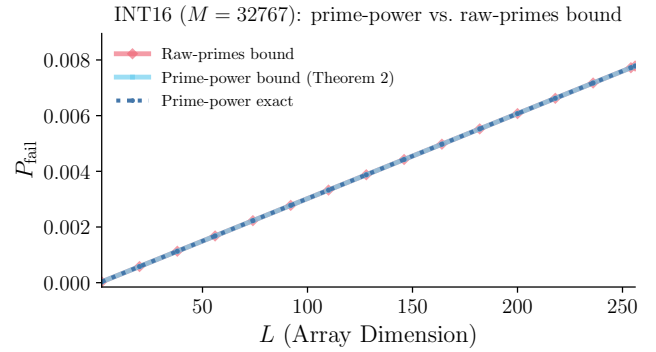


(b) Ambiguous multiple count in the sketch vector across array dimensions L ; p_L is the additional entry added to the test vector at each L . The prime-power pool yields far fewer ambiguous multiples than raw primes, reducing false localization candidates and P_{fail} as seen above.

Figure 2: Raw primes vs. prime-power coprimes for INT8 ($M = 127$). Beyond $L = 27$, small primes enter the raw-prime pool, raising the ambiguous multiple count; more error values become indistinguishable from the true fault, introducing false localization candidates and increasing P_{fail} ; the union bound also overcounts for raw primes, with the exact value falling below it.



(a) INT8 ($M = 127$, $\pi(127) = 31$): gap is most pronounced near $L = 31$, where the raw-prime pool is forced to include small primes with many multiples in $\{1, \dots, M\}$.



(b) INT16 ($M = 32767$, $\pi(32767) = 3512$): all curves remain negligible for $L \leq 256$, confirming single-round sufficiency.

Figure 3: Prime-power exact (blue dotted), prime-power bound (cyan, Theorem 2), and raw-primes bound (rose) for INT8 and INT16. The prime-power exact and bound coincide in both cases, confirming no overcounting.

Single-bit-error model. By Remark 3, using the 30 odd primes (3 through 127) guarantees exact localization in one round for any error $e = \pm 2^\beta$.

Cross-precision comparison. Precision has a large effect on localization reliability: the pool size difference ($\pi(127) = 31$ vs. $\pi(32767) = 3512$) means that, at any given array dimension, INT16 achieves substantially lower P_{fail} than INT8. Concretely, INT8 reaches $P_{\text{fail}} \approx 0.534$ at its pool boundary ($L = 31$), while INT16 remains below 0.008 even at $L = 256$, as shown in Figures 3a and 3b.

5.2 Empirical Results

Experiments are run on a custom Python cycle-accurate simulator using weights from the `model.layers.0.mlp.down_proj` tensor of Qwen2.5-0.5B [48]. We also measure P_{fail} empirically across array dimensions, and characterize the cycle cost of the sketch vector pass for both the one-round and two-round schemes using SCALE-Sim 3.0.0 [10].

5.2.1 Empirical Validation of P_{fail} . For each array dimension L and precision, a fresh L -row weight-stationary systolic array is instantiated and loaded with the first L rows of `model.layers.0.mlp.down_proj` of Qwen2.5-0.5B [48] (full tensor shape 896×4864): for INT8, weights are taken from the W8A8 quantized version `neuralmagic/Qwen2.5-0.5B-Instruct-quantized.w8a8`, stored as signed 8-bit integers; for INT16, from the BF16 version `Qwen/Qwen2.5-0.5B-Instruct`, quantized to signed 16-bit integers.⁴ For each of the 500 trials, the fault row $i^* \in \{0, \dots, L-1\}$, fault column $j^* \in \{0, \dots, K-1\}$, and error magnitude $e \in \{1, \dots, M\}$ are sampled uniformly at random; the sketch vector is constructed from the prime-power pool for the corresponding precision (Section 4.3). An additive fault of size e is injected into the Wreg of PE (i^*, j^*) , the prime-power coprime sketch vector is passed through the faulty

⁴The weights do not enter the P_{fail} computation: localization is determined entirely by the syndrome $x_{j^*} \cdot e$. Therefore, only the precision of the random error e and the sketch vector affect P_{fail} , through the magnitude range $\{1, \dots, M\}$ they induce, and not the precision or values of the weight matrix. This was validated using the custom cycle-accurate Python simulator.

array, and the candidate row set is recovered from the output syndrome.

Localization is incomplete when, in addition to i^* , at least one other row appears in the candidate set of Algorithm 1. The empirical failure rate is compared against the Theorem 2 prime-power bound. We sweep $L \in \{4, 8, 16, 31, 40, 50, 60\}$ for INT8 and $L \in \{4, 8, 16, 32, 64, 128, 256\}$ for INT16.

Figures 4a and 4b report results for the INT8 ($M = 127$) and INT16 ($M = 32767$) error domains respectively. The shaded band around each simulation curve shows the 95% confidence interval [49] for the 500-trial sample. For INT8, the empirical rate tracks the Theorem 2 bound closely across all tested dimensions; for $L > 31 = \pi(127)$ the prime-power pool is exhausted and both the Theorem 2 bound and the exact P_{fail} saturate to 1 analytically, though the empirical failure rate degrades more gradually (discussed below), motivating the two-round scheme of Section 4.4. Occasional crossings where the empirical estimate slightly exceeds the bound are expected: the bound is a guarantee on the true average P_{fail} , while the empirical estimate from a finite number of trials is subject to sampling noise, so small upward fluctuations do not contradict the theoretical guarantee. For INT16 the failure rate is negligible across all practical array sizes, confirming that the prime-power construction provides reliable single-round localization up to 256×256 arrays at higher precision.

Graceful degradation beyond the pool boundary. A closer look at the INT8 curve reveals that the empirical P_{fail} remains noticeably below 1 for L slightly above 31. Both the Theorem 2 union bound and the exact P_{fail} (Appendix A) saturate to 1 as soon as $L > \pi(127) = 31$ because entry/prime-factor repetition is unavoidable, but repetition does not affect every row equally: for $L = 31 + k$, exactly k rows must share a prime-power entry with another row, while the remaining $31 - k$ rows still carry unique entries. Since the fault location i^* is drawn uniformly over all L rows, the probability that it falls on a non-repeated row is $(31 - k)/L$, and single-round localization succeeds in those cases. The empirical P_{fail} therefore rises by at most $2k/L$ due to entry repetition, rather than jumping immediately to 1. Concretely, for $L = 32$ ($k = 1$), exactly $2/32$ of fault locations fall on shared-entry rows and fail with certainty; the remaining $30/32$ still benefit from single-round localization. This graceful degradation is practically useful: INT8 arrays moderately larger than 31 rows can still benefit from single-round FLARE localization for the majority of fault locations, and the two-round fallback is only strictly necessary once enough rows carry repeated entries to meaningfully raise the overall failure rate.

5.2.2 Cycle Overhead. We measure the cycle cost of issuing the sketch vector(s) relative to a standard inference tile, for both the one-round and two-round schemes across array dimensions. In the ISA-integrated deployment model (Section 4.5), the weights for the tile under test are already resident in the PEs when the sketch vector is issued. The relevant overhead is therefore the *incremental* cost of issuing the sketch vector through the already-loaded array. The sketch vector is $1 \times L$, one element per PE column of the $L \times L$ array, making a sketch pass a GEMM of shape $(L \times L) \times (L \times 1)$.

We measure this using SCALE-Sim 3.0.0 [10]. The Baseline column of Table 3 reports the cycle count for one inference tile (including weight loading) as measured by SCALE-Sim; this is subtracted

Table 3: Incremental cycle overhead of FLARE on an $L \times L$ Weight-Stationary array, measured with SCALE-Sim 3.0.0 [10]. The sketch vector is $1 \times L$; Util.(%) is the PE utilization of the baseline run (fraction of PE-cycles actively performing a MAC, as reported by SCALE-Sim); Overhead % = $\Delta\text{cycles}/\text{baseline} \times 100$.

L	Baseline	Util.(%)	1-round		2-round	
			cyc.	%	cyc.	%
8	554	3.45	1	0.18	2	0.36
16	586	1.64	1	0.17	2	0.34
32	650	0.80	1	0.15	2	0.31
64	778	0.40	1	0.13	2	0.26
128	2606	0.20	1	0.04	2	0.08
256	7836	0.10	1	0.01	2	0.03

from the total cycle count with the sketch vector to isolate the test overhead alone. For the two round scheme both sketch vectors are issued back-to-back against the same baseline.

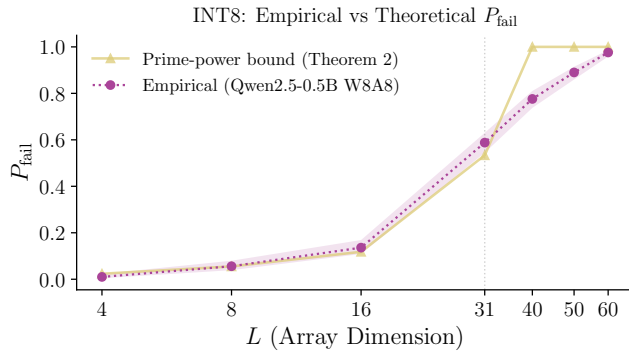
Table 3 reports the results. The sketch vector has the same length as the array column count and the pipeline absorbs each additional vector in exactly **1 cycle**, regardless of array size. The two round scheme therefore costs 2 cycles total. At 128×128 and 256×256 the single-round overhead is 0.04% and 0.01% respectively; the two-round overhead is 0.08% and 0.03%. The post-pipeline detection work (syndrome subtraction and $O(L)$ divisibility checks) runs asynchronously on the adjacent array controller and can overlap with subsequent tile computation. The fault-identification latency is $O(L)$ controller clock cycles; whether this overlaps fully with array execution depends on the controller’s arithmetic throughput, which is implementation-specific and not characterized here. The reported cycle counts therefore reflect only the array-side cost of issuing the sketch vector(s).

6 Conclusion

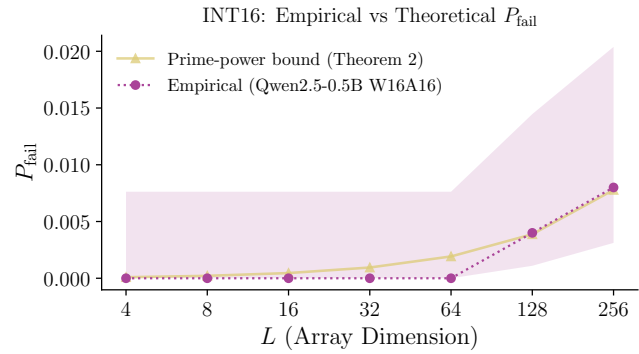
We presented FLARE, a lightweight algorithmic framework for PE-level fault localization in systolic arrays without hardware redundancy. By leveraging pairwise coprime test vectors, FLARE encodes fault location into algebraic divisibility signatures that survive systolic accumulation, overcoming the fundamental limitation of prior approaches that only achieve column-level detection. We show that a single test pass localizes faults with miss probability bounded by Theorem 2 under a general bounded error model, while a two round ratio-based extension guarantees exact localization for all practical array sizes. Importantly, FLARE requires no architectural modifications and integrates seamlessly with existing execution pipelines. Experimental results demonstrate near-perfect localization for INT16 and strong guarantees for INT8, with test overhead under 1% of a single GEMM tile, making it practical for in-field deployment. Overall, FLARE highlights the potential of algorithm-hardware co-design for low-cost, software-defined fault diagnosis in AI accelerators.

Acknowledgments

We acknowledge NSF awards #2506573 and #2516418 for this work. We acknowledge Prof. Tushar Krishna at Georgia Tech ECE for helpful discussions. We also thank Ajay Sharma Mandadi at Georgia Tech for valuable feedback throughout this work.



(a) INT8 ($M = 127$): For $L > 31 = \pi(127)$ the prime-power pool is exhausted and the analytical P_{fail} saturates to 1, though the empirical rate rises gradually as non-repeated entries continue to localize successfully for sizes moderately beyond the boundary.



(b) INT16 ($M = 32767$): The failure rate remains negligible across all tested dimensions, consistent with the Theorem 2 bound.

Figure 4: Empirical P_{fail} versus array dimension L for INT8 and INT16 with Theorem 2 prime-power bound (500 trials; Qwen2.5-0.5B weights: W8A8 for INT8, BF16 quantized to INT16 for INT16); shaded regions denote 95% confidence bands [49].

References

- [1] Norman P Jouppi, Cliff Young, Nishant Patil, David Patterson, Gaurav Agrawal, Raminder Bajwa, Sarah Bates, Suresh Bhatia, Nan Boden, Al Borchers, et al. In-dataloader performance analysis of a tensor processing unit. In *Proceedings of the 44th annual international symposium on computer architecture*, pages 1–12, 2017.
- [2] Lei Deng, Guoqi Li, Song Han, Luping Shi, and Yuan Xie. Model compression and hardware acceleration for neural networks: A comprehensive survey. *Proceedings of the IEEE*, 108(4):485–532, 2020.
- [3] Yubin Qin, Yang Wang, Zhiren Zhao, Xiaolong Yang, Yang Zhou, Shaojun Wei, Yang Hu, and Shouyi Yin. Mecla: Memory-compute-efficient LLM accelerator with scaling sub-matrix partition. In *2024 ACM/IEEE 51st Annual International Symposium on Computer Architecture (ISCA)*, pages 1032–1047. IEEE, 2024.
- [4] Zishen Wan, Hanchen Yang, Ritik Raj, Che-Kai Liu, Ananda Samajdar, Arijit Raychowdhury, and Tushar Krishna. CogSys: Efficient and scalable neurosymbolic cognition system via algorithm-hardware co-design. In *2025 IEEE International Symposium on High Performance Computer Architecture (HPCA)*, pages 775–789. IEEE, 2025.
- [5] Peter H. Hochschild, Paul Turner, Jeffrey C. Mogul, Rama Gober, Parthasarathy Ranganathan, David E. Culler, and Amin Vahdat. Cores that don't count. In *Proceedings of the Workshop on Hot Topics in Operating Systems (HotOS)*, pages 9–16. ACM, 2021.
- [6] Harish Dattatraya Dixit, Sneha Pendharkar, Matt Beadon, Chris Mason, Tejasvi Chakravarthy, Bharath Muthiah, and Sriram Sankar. Silent data corruptions at scale. In *arXiv preprint arXiv:2102.11245*, 2021.
- [7] Yi He, Mike Hutton, Steven Chan, Robert De Gruijl, Rama Govindaraju, Nishant Patil, and Yanjing Li. Understanding permanent hardware failures in deep learning training accelerator systems. In *2023 IEEE European Test Symposium (ETS)*, pages 1–6. IEEE, 2023.
- [8] Jeff Jun Zhang, Tianyu Gu, Kanad Basu, and Siddharth Garg. Analyzing and mitigating the impact of permanent faults on a systolic array based neural network accelerator. In *2018 IEEE 36th VLSI Test Symposium (VTS)*, pages 1–6. IEEE, 2018.
- [9] H. T. Kung and Charles E. Leiserson. Systolic arrays for VLSI. *Computer*, 15(1):37–46, 1982.
- [10] Ritik Raj, Sarbartha Banerjee, Nikhil Chandra, Zishen Wan, Jianming Tong, Ananda Samajdhar, and Tushar Krishna. SCALE-Sim v3: A modular cycle-accurate systolic accelerator simulator for end-to-end system analysis. In *2025 IEEE International Symposium on Performance Analysis of Systems and Software (ISPASS)*, pages 186–200. IEEE, 2025.
- [11] Kuang-Hua Huang and Jacob A. Abraham. Algorithm-based fault tolerance for matrix operations. *IEEE Transactions on Computers*, C-33(6):518–528, 1984.
- [12] Cristian Constantinescu. Trends and challenges in VLSI circuit reliability. *IEEE Micro*, 23(4):14–19, 2003.
- [13] Bruno F Goldstein, Victor C Ferreira, Sudarshan Srinivasan, Dipankar Das, Alexandre S Nery, Sandip Kundu, and Felipe MG França. A lightweight error-resiliency mechanism for deep neural networks. In *2021 22nd International Symposium on Quality Electronic Design (ISQED)*, pages 311–316, Santa Clara, CA, USA, 2021. IEEE.
- [14] Sandeep Bal, Chandra Sekhar Mummidi, Victor Da Cruz Ferreira, Sudarshan Srinivasan, and Sandip Kundu. A novel fault-tolerant architecture for tiled matrix multiplication. In *2023 Design, Automation & Test in Europe Conference & Exhibition (DATE)*, pages 1–6, Antwerp, Belgium, 2023. IEEE.
- [15] Natalia Cherezova, Artur Jutman, and Maksim Jenihhin. FORTALESA: Fault-tolerant reconfigurable systolic array for DNN inference. *Microprocessors and Microsystems*, page 105222, 2025.
- [16] Hayoung Lee, Jongho Park, and Sungho Kang. An area-efficient systolic array redundancy architecture for reliable AI accelerator. *IEEE Transactions on Very Large Scale Integration (VLSI) Systems*, 32(10):1950–1954, 2024.
- [17] Keewon Cho, Ingeol Lee, Hyeonchan Lim, and Sungho Kang. Efficient systolic-array redundancy architecture for offline/online repair. *Electronics*, 9(2):338, 2020.
- [18] Yingnan Zhao, Ke Wang, and Ahmed Lourri. FSA: An efficient fault-tolerant systolic array-based DNN accelerator architecture. In *2022 IEEE 40th International Conference on Computer Design (ICCD)*, pages 545–552. IEEE, 2022.
- [19] Youssef Ait Alama, Sampada Sakpal, Ke Wang, Razvan Bunescu, Avinash Karanth, and Ahmed Lourri. Algorithmic strategies for sustainable reuse of neural network accelerators with permanent faults. In *2025 IEEE International Symposium on Defect and Fault Tolerance in VLSI and Nanotechnology Systems (DFT)*, pages 1–6. IEEE, 2025.
- [20] Hayoung Lee, Jihye Kim, Jongho Park, and Sungho Kang. STRAIT: Self-test and self-recovery for AI accelerator. *IEEE Transactions on Computer-Aided Design of Integrated Circuits and Systems*, 42(9):3092–3104, 2023.
- [21] Wei-Kai Liu, Jonti Talukdar, Benjamin Tan, and Krishnendu Chakraborty. Runtime fault localization in deep neural network accelerators. *ACM Transactions on Design Automation of Electronic Systems*, 31(1):1–27, 2025.
- [22] Umair Saeed Solangi, Muhammad Ibtesam, Muhammad Adil Ansari, Jinuk Kim, and Sungju Park. Test architecture for systolic array of edge-based AI accelerator. *IEEE Access*, 9:96700–96710, 2021.
- [23] Eleonora Vacca, Giorgio Ajmone, and Luca Sterpone. RunSAFER: A novel runtime fault detection approach for systolic array accelerators. In *2023 IEEE 41st International Conference on Computer Design (ICCD)*, pages 596–604, Washington, DC, USA, 2023. IEEE.
- [24] Christodoulos Peltekis, Chrysostomos Nicopoulos, and Giorgos Dimitrakopoulos. Periodic online testing for sparse systolic tensor arrays. In *2025 14th International Conference on Modern Circuits and Systems Technologies (MOCASST)*, pages 1–6. IEEE, 2025.
- [25] Fabiano Libano, Paolo Rech, and John Brunhaver. Efficient error detection for matrix multiplication with systolic arrays on FPGAs. *IEEE Transactions on Computers*, 72(8):2390–2403, 2023.
- [26] Claus Braun, Sebastian Halder, and Hans Joachim Wunderlich. A-ABFT: Autonomous algorithm-based fault tolerance for matrix multiplications on graphics processing units. In *2014 44th Annual IEEE/IFIP International Conference on Dependable Systems and Networks*, pages 443–454. IEEE, 2014.
- [27] Mehdi Safarpour, Reza Inanlou, and Olli Silvén. Algorithm level error detection in low voltage systolic array. *IEEE Transactions on Circuits and Systems II: Express Briefs*, 69(2):569–573, 2021.
- [28] Xinghua Xue, Cheng Liu, Feng Min, Tao Luo, and Yinhe Han. ApproxABFT: Approximate algorithm-based fault tolerance for neural network processing. *arXiv preprint arXiv:2302.10640*, 2023.
- [29] Haoxuan Liu, Vasu Singh, Michał Filipiuk, and Siva Kumar Sastry Hari. ALBERTA: Algorithm-based error resilience in transformer architectures. *IEEE Open Journal of the Computer Society*, 6:85–96, 2024.

- [30] Kwondo Ma, Chandramouli Amarnath, and Abhijit Chatterjee. Error resilient transformers: A novel soft error vulnerability guided approach to error checking and suppression. In *2023 IEEE European Test Symposium (ETS)*, pages 1–6. IEEE, 2023.
- [31] Tong Xie, Jiawang Zhao, Zishen Wan, Zuodong Zhang, Yuan Wang, Runsheng Wang, Ru Huang, and Meng Li. ReaLM: Reliable and efficient large language model inference with statistical algorithm-based fault tolerance. *arXiv preprint arXiv:2503.24053*, 2025.
- [32] James L Massey and Oscar N Garcia. Error-correcting codes in computer arithmetic. In *Advances in Information Systems Science: Volume 4*, pages 273–326. Springer, 1972.
- [33] Sorin Iacobovici. Residue based error detection for integer and floating point execution units, August 18 2015. US Patent 9,110,768.
- [34] Jingweijia Tan, Qixiang Wang, Kaige Yan, Xiaohui Wei, and Xin Fu. SACA-FI: A microarchitecture-level fault injection framework for reliability analysis of systolic array based CNN accelerator. *Future Generation Computer Systems*, 147:251–264, 2023.
- [35] Mahdi Taheri, Masoud Daneshlatab, Jaan Raik, Maksim Jenihhin, Salvatore Pappalardo, Paul Jimenez, Bastien Deveautour, and Alberto Bosio. SAFFIRA: a framework for assessing the reliability of systolic-array-based DNN accelerators. In *2024 27th International Symposium on Design & Diagnostics of Electronic Circuits & Systems (DDECS)*, pages 19–24. IEEE, 2024.
- [36] Shamik Kundu, Suvadeep Banerjee, Arnab Raha, Suriyaprakash Natarajan, and Kanad Basu. DiagNNose: Toward error localization in deep learning hardware-based on VTA-TVM stack. *IEEE Transactions on Computer-Aided Design of Integrated Circuits and Systems*, 43(1):217–229, 2023.
- [37] Guanpeng Li, Siva Kumar Sastry Hari, Michael Sullivan, Timothy Tsai, Karthik Pattabiraman, Joel Emer, and Stephen W. Keckler. Understanding error propagation in deep learning neural network (DNN) accelerators and applications. In *Proceedings of the International Conference for High Performance Computing, Networking, Storage and Analysis (SC)*, 2017.
- [38] Sanghyun Hong, Pietro Frigo, Yiğitcan Kaya, Cristiano Giuffrida, and Tudor Dumitras. Terminal brain damage: Exposing the graceless degradation in deep neural networks under hardware fault attacks. In *Proceedings of the 28th USENIX Security Symposium*, 2019.
- [39] Le-Ha Hoang, Muhammad Abdullah Hanif, and Muhammad Shafique. FT-ClipAct: Resilience analysis of deep neural networks and improving their fault tolerance using clipped activation. In *2020 Design, Automation & Test in Europe Conference & Exhibition (DATE)*, pages 1241–1246. IEEE, 2020.
- [40] Elbruz Ozen and Alex Orailoglu. Just say zero: Containing critical bit-error propagation in deep neural networks with anomalous feature suppression. In *Proceedings of the 39th International Conference on Computer-Aided Design*, pages 1–9, 2020.
- [41] Zishen Wan, Nandhini Chandramoorthy, Karthik Swaminathan, Pin-Yu Chen, Vijay Janapa Reddi, and Arijit Raychowdhury. Berry: Bit error robustness for energy-efficient reinforcement learning-based autonomous systems. In *2023 60th ACM/IEEE Design Automation Conference (DAC)*, pages 1–6. IEEE, 2023.
- [42] Zitao Chen, Guanpeng Li, and Karthik Pattabiraman. A low-cost fault corrector for deep neural networks through range restriction. In *2021 51st Annual IEEE/IFIP International Conference on Dependable Systems and Networks (DSN)*, pages 1–13. IEEE, 2021.
- [43] Elbruz Ozen and Alex Orailoglu. Boosting bit-error resilience of DNN accelerators through median feature selection. *IEEE Transactions on Computer-Aided Design of Integrated Circuits and Systems*, 39(11):3250–3262, 2020.
- [44] Xun Jiao, Fred Lin, Harish D. Dixit, Joel Coburn, Abhinav Pandey, Han Wang, Venkat Ramesh, Jianyu Huang, Wang Xu, Daniel Moore, and Sriram Sankar. PVF (parameter vulnerability factor): A scalable metric for understanding AI vulnerability against SDCs in model parameters. *arXiv preprint arXiv:2405.01741*, 2024.
- [45] Florian Geissler, Syed Qutub, Michael Paulitsch, and Karthik Pattabiraman. A low-cost strategic monitoring approach for scalable and interpretable error detection in deep neural networks. In *International Conference on Computer Safety, Reliability, and Security*, pages 75–88. Springer, 2023.
- [46] G. H. Hardy and E. M. Wright. *An Introduction to the Theory of Numbers*. Oxford University Press, 6th edition, 2008.
- [47] Ron M. Roth. *Introduction to Coding Theory*. Cambridge University Press, 2006.
- [48] An Yang, Anfeng Li, Baosong Yang, Beichen Zhang, Binyuan Hui, Bo Zheng, Bowen Yu, Chang Gao, Chengen Huang, Chenxu Lv, et al. Qwen3 technical report. *arXiv preprint arXiv:2505.09388*, 2025.
- [49] Edwin B Wilson. Probable inference, the law of succession, and statistical inference. *Journal of the American Statistical Association*, 22(158):209–212, 1927.

A Exact Probability via Inclusion-Exclusion

The bound of Theorem 2 applies the union bound, summing $\lfloor M/x_k \rfloor$ over all rows $k \neq i^*$. This can overcount when e is simultaneously

divisible by more than one pool entry – for example, $e = 6$ is divisible by both $x = 2$ and $x = 3$, thus counted twice, even though it corresponds to a single failure event. The exact average P_{fail} corrects for this via the inclusion-exclusion principle.

Setup. Localization is incomplete when at least one row $k \neq i^*$ survives the divisibility test. The syndrome at the faulty column is $\Delta = e \cdot x_{i^*}$, so row k passes the test when $x_k \mid e \cdot x_{i^*}$; since pool entries are pairwise coprime ($\gcd(x_k, x_{i^*}) = 1$ for $k \neq i^*$), this simplifies to $x_k \mid e$. Since e is bounded by the precision range $\{1, \dots, M\}$, the failure-inducing values are precisely the multiples of x_k within this range: the errors that render row k indistinguishable from i^* .

Let $A_k = \{e \in \{1, \dots, M\} : x_k \mid e\}$ be the set of such errors for row k . Taking the union over all rows $k \neq i^*$ collects all errors that would cause at least one wrong row to survive alongside the true faulty row. For a fixed faulty row i^* :

$$P_{\text{fail}}(i^*) = \frac{1}{M} \left| \bigcup_{k \neq i^*} A_k \right|. \quad (10)$$

Inclusion-exclusion formula. Let S denote a non-empty subset of non-faulty row indices drawn from $\{1, \dots, L\} \setminus \{i^*\}$; each such subset represents a combination of rows that would simultaneously pass the divisibility test, and its contribution counts the errors $e \leq M$ divisible by all entries x_k for $k \in S$, i.e., $|\bigcap_{k \in S} A_k| = \lfloor M / \prod_{k \in S} x_k \rfloor$. Summing with alternating signs over all such subsets gives the exact union cardinality:

$$\left| \bigcup_{k \neq i^*} A_k \right| = \sum_{j=1}^{L-1} (-1)^{j+1} \sum_{\substack{S \subseteq \{1, \dots, L\} \setminus \{i^*\} \\ |S|=j}} \left\lfloor \frac{M}{\prod_{k \in S} x_k} \right\rfloor. \quad (11)$$

Averaging (11) uniformly over $i^* \in \{1, \dots, L\}$ gives the average exact P_{fail} , plotted as *exact* in Figures 2 and 3.

Prime-power pool. For the prime-power pool, all pairwise products $x_j x_k$ exceed M , so no $e \leq M$ is simultaneously divisible by two distinct entries and overcounting cannot occur. Consequently, formula (11) collapses to the union bound of Theorem 2: the bound and exact value coincide, justifying its use throughout the paper.

Computational complexity. The summation in (11) ranges over all non-empty subsets of $\{1, \dots, L\} \setminus \{i^*\}$, where every subset is formed by choosing elements in all possible combinations. Since the faulty row i^* is excluded from subset formation, there are $L - 1$ non-faulty rows to choose from. The number of subsets of size j from these $L - 1$ rows is $\binom{L-1}{j} = \frac{(L-1)!}{j!(L-1-j)!}$, and the total number of non-empty subsets across all sizes is $\sum_{j=1}^{L-1} \binom{L-1}{j} = 2^{L-1} - 1$ by the binomial theorem, which grows exponentially in L .

For each subset S of size j , computing the product $\prod_{k \in S} x_k$ costs $O(j \log M)$ bit operations and the subsequent floor division costs $O(\log M)$. Averaging over all L choices of i^* multiplies the total cost by L , giving $O(L \cdot 2^L \cdot \log M)$ bit operations overall. In contrast, the Theorem 2 union bound requires only $O(L)$ floor divisions totalling $O(L \log M)$, independent of the subset structure. For large L the exact formula is therefore computationally prohibitive, further supporting the use of the union bound in practice.